Stem Cell Research 15 (2015) 243–253

Contents lists available at ScienceDirect

Stem Cell Research

journal homepage: www.elsevier.com/locate/scr

Longitudinal tracking of triple labeled umbilical cord derived mesenchymal stromal cells in a mouse model of Amyotrophic Lateral Sclerosis

Martina Bruna Violatto [a,*], Chiara Santangelo [a], Chiara Capelli [b], Roberta Frapolli [a], Raffaele Ferrari [a], Leopoldo Sitia [a], Massimo Tortarolo [a], Laura Talamini [a], Sara Previdi [a], Davide Moscatelli [c], Mario Salmona [a], Martino Introna [b], Caterina Bendotti [a], Paolo Bigini [a]

[a] IRCCS — Istituto di Ricerche Farmacologiche "Mario Negri", Milano, Italy
[b] USS Centro di Terapia Cellulare "G. Lanzani", A. O. Papa Giovanni XXIII, Bergamo, Italy
[c] Dipartimento di Chimica, Materiali e Ingegneria Chimica "G. Natta", Politecnico di Milano, Milano, Italy

ARTICLE INFO

Article history:
Received 17 April 2015
Received in revised form 25 May 2015
Accepted 26 June 2015
Available online 27 June 2015

Keywords:
Mesenchymal stromal cells
Umbilical cord
Amyotrophic Lateral Sclerosis
Cell tracking
Nanotechnology
In vivo imaging

ABSTRACT

The translational potential of cell therapy to humans requires a deep knowledge of the interaction between transplanted cells and host tissues. In this study, we evaluate the behavior of umbilical cord mesenchymal stromal cells (UC-MSCs), labeled with fluorescent nanoparticles, transplanted in healthy or early symptomatic transgenic SOD1G93A mice (a murine model of Amyotrophic Lateral Sclerosis). The double labeling of cells with nanoparticles and Hoechst-33258 enabled their tracking for a long time in both cells and tissues. Whole-body distribution of UC-MSCs was performed by in-vivo and ex-vivo analyses 1, 7, 21 days after single intravenous or intracerebroventricular administration. By intravenous administration cells were sequestered by the lungs and rapidly cleared by the liver. No difference in biodistribution was found among the two groups. On the other hand, UC-MSCs transplanted in lateral ventricles remained on the choroid plexus for the whole duration of the study even if decreasing in number. Few cells were found in the spinal cord of SOD1G93A mice exclusively. No migration in brain parenchyma was observed. These results suggest that the direct implantation in brain ventricles allows a prolonged permanence of cells close to the damaged areas and makes this method of tracking reliable for future studies of efficacy.

1. Introduction

Over the last two decades, cell-based therapy has been evaluated in cardiovascular, oncologic, autoimmune and neurodegenerative diseases. In the neurological field preclinical studies have demonstrated the potential of stem cell injection (Lindvall and Kokaia, 2006). On the other hand, their clinical application is still limited and controversial (Viswanathan and Keating, 2011). Thanks to their self-renewal and differentiation abilities, stem cells had been originally considered as a possible tool to replace damaged cells by an initial selective migration to the injured area and a subsequent differentiation into the affected neurons (Bjorklund and Lindvall, 2000). Unfortunately, this fascinating mechanism of repair rapidly faded away and the hope of an effective care for neurodegenerative disorders by topic transplantation of highly committed neural stem cells and/or embryonic totipotential cells was more and more neglected. On the contrary, there are growing evidences of an alternative endocrine-like mechanism of action of stem cells in different murine models of acute and chronic neurological disorders that does not involve any specific cell differentiation toward the neural lineage (Silani et al., 2010; Uccelli et al., 2011, 2012). This mechanism, commonly referred as bystander effect, is mainly based on the secretion of trophic factors, anti-inflammatory cytokines, immunomodulatory agents and soluble molecules even far from the diseased area by transplanted cells. This experimental evidence greatly enlarged the spectrum of potential cell candidates, in particular stromal cells derived from extra-embryonic tissues, and paved the way to alternative systemic routes of administrations, in addition to the intraparenchyma implantation (Corti et al., 2004; Zhao et al., 2007; Knippenberg et al., 2012a; Mitrecic et al., 2010; Willing et al., 2008). The possibility to perform preclinical studies by systemically injecting cells in the bloodstream (IV) or, more locally intracerebroventricularly (ICV), has been adopted in many models of neurodegenerative disorders. All these premises prompted the scientific community to focus the attention on the effect of

* Corresponding author at: Martina Bruna Violatto, IRCCS — Istituto di Ricerche Farmacologiche "Mario Negri", Dipartimento di Biochimica e Farmacologia Molecolare, Via La Masa 19, 20156 Milano, Italia.
E-mail address: martina.violatto@marionegri.it (M.B. Violatto).

http://dx.doi.org/10.1016/j.scr.2015.06.010

systemically injected fetal stem cells in different models of neurodegenerative disorders. In particular a large number of studies have been recently carried out in mouse models of Amyotrophic Lateral Sclerosis (ALS).

ALS is a fatal neurodegenerative disorder characterized by a selective and widespread degeneration of lower and upper motor neurons (Gordon, 2013; Rowland and Shneider, 2001). The main symptomatic features of ALS are muscular atrophy, motor paralysis and difficulties in speaking, swallowing, chewing and breathing (Harms and Baloh, 2013). Respiratory failure is the most common cause of death for ALS patients, which occurs within 3–5 years from the diagnosis (Al-Chalabi and Hardiman, 2013). The effect of Riluzole, the only drug approved by the Food and Drug Administration more than twenty years ago is very modest in prolonging the life of patients without ameliorating their quality of life, even lower than palliative cares (e.g. tracheostomy and invasive ventilation) (Cheah et al., 2010; Musaro, 2013). For these reasons, alternative and innovative therapeutic strategies are strongly and urgently required. Interestingly, it has been recently reported that both the ICV and the IV infusions of ematopoietic and mesenchymal stem cells induced a protective effect in two different models of ALS. Since no clear localization of stem cells within the areas of degenerating motor neurons was found, it was suggested that this was likely the response to the production of anti-inflammatory and immunomodulatory factors produced by the stem cells even far from the damaged areas (Garbuzova-Davis et al., 2008; Canzi et al., 2012; Bigini et al., 2011).

However what is the fate of the cells in terms of biodistribution, organ accumulation, potential target migration and clearance after a systemic or ICV administration(s) is not clearly defined due to the lack of proper markers to track these cells in both healthy and diseased experimental subjects.

Different strategies to follow the fate of transplanted stem cells in preclinical models of human disorders have been reported (Wang and Moore, 2012). In particular, the FDA approved Superparamagnetic Iron Oxide nanoparticles (SPIOn) can provide an easily transferable and non-invasive system to follow stem cells using magnetic resonance imaging. An innovative approach to further increase the reliability of stem cells tracking in different murine models of ALS by specifically labeling the cytoplasm with SPIOn and the nucleus with Hoechst-33258 has been developed by our group (Canzi et al., 2012; Bigini et al., 2012). Although this strategy enabled us to determine the interaction of various types of fetal stem cells in several models of motor neuron degeneration at different times points, perplexities were raised about the biocompatibility and the lack of cell perturbation after SPIOn internalization (Calero et al., 2014; Li et al., 2013; Reddy et al., 2012). To overcome this problem, fluorescent, biocompatible and long lasting traceable poly (methyl methacrylate) nanoparticles (PMMA-NPs) have been recently developed for the tracking of human amniotic fluid cells by ex-vivo analyses. The reliability of our approach was furthermore evaluated by in-vivo studies where the co-incubation of SPIOn and PMMA-NPs confirmed the presence of the two tracers in transplanted cells for at least three weeks after administration (Cova et al., 2013). On the basis of these results in the present study we proposed to label human umbilical cord mesenchymal stromal cells (UC-MSCs) with PMMA-NPs, that segregate into the cytoplasm, and with the nuclear dye Hoechst-33258 before to inject them ICV or intravenously in both healthy and early symptomatic SOD1G93A mice in order to track them at different time points during the disease progression. UC-MSCs were selected because they represent an innovative pool of MSCs, with a simpler, safer and cheaper collection from donors compared to the bone marrow stem cells and the cord blood mononuclear cells. In addition, mesenchymal stromal cells have shown a strong immunomodulatory and cyto-protective activity in different preclinical models of acute inflammation (Griffin et al., 2013; Stagg and Galipeau, 2013; Uccelli et al., 2008). To optimize the tracking procedures cells were labeled with PMMA-NPs, that segregate into the cytoplasm, and with the nuclear dye Hoechst-33258. Two different fluorophores, Rhodamine B (RhB) and a deep infrared dye (DIR) respectively, were conjugated to NPs in order to combine in-vivo and ex-vivo analyses. The labeling enabled us to follow the fate of systemically administered UC-MSCs for a prolonged temporal window that was hypothesized sufficient for the cells to exert a therapeutic response in SOD1G93A mice. This is the first example in preclinical ALS studies in which the tracking of the same type of stem cells is reported by using two different ways of administration and where this longitudinal tracking has been carried out in living mice by whole body scanning with optical imaging system. The results obtained by this work can be therefore considered as a robust pre-requisite to plan future experiments in which the cell-host interaction could be easily correlated with the therapeutic efficacy, in a sort of theranostic approach, independently of the pathological model or the cell-type utilized.

2. Materials and methods

2.1. Nanoparticles synthesis and characterization

Poly (methyl methacrylate) nanoparticles (PMMA-NPs) were used to label stem cells thanks to their biocompatibility and to their low level of biodegradability (Cova et al., 2013). They were obtained from a co-polymerization between methyl methacrylate (MMA) and a macromonomer of 2-hydroxyethyl methacrylate (HEMA) covalently bound to RhB, through an emulsion free-radical polymerization process. DIR was not loaded during NP formation due to high temperature and to the presence radicals; therefore a post-synthesis process has been adopted (Sitia et al., 2014).

For our investigation the following nanoparticles have been synthesized:

- Positive 50 nm PMMA-NPs (number of NPs/ml $H_2O = 2.01E * 10^{14}$; polymer concentration = 50 mg/ml)
- Positive 200 nm PMMA-NPs (number of NPs/ml $H_2O = 4.62E * 10^{12}$; polymer concentration = 50 mg/ml)

Details on synthesis and NP characterization are reported in our previous study (Sitia et al., 2014).

2.2. UC collection and cell culture

Fresh human umbilical cords (UC) were collected from the Operating Room of the Obstetrics and Gynecology Unit at A.O. Papa Giovanni XXIII in Bergamo (Italy). Informed written consent was obtained from each donor mother according to the guidelines of ethical committee of the A.O. Papa Giovanni XXIII, as required by the clinical trial "Umbilical Cord Derived Mesenchymal Stromal Cells For The Treatment of Severe Steroid-resistant Graft Versus Host Disease" (clinicaltrials.gov ID NCT02032446) approved by "Istituto Superiore di Sanità" and "Agenzia Italiana del Farmaco". After cesarean sections, UC-MSCs have been isolated from whole UC by tissue mechanical disaggregation and cultivated as previously described (Capelli et al., 2011). Briefly, the UCs were cut into 5 cm long segments which were longitudinally cut and split open to expose the inner surface. Each UC segment, subsequently minced in very small fragments, was transferred into 150 mm cell culture Petri dishes (Corning) containing MSC expansion medium consisting of alpha-Minimum Essential Medium (MEM) (Life-Technologies) enriched with 5% human platelet lysate obtained from healthy donors, 50 μg/ml gentamicin (Fisiopharma) and 2 UI/ml Heparin (Hospira). They were maintained at 37 °C in a humidified atmosphere with 5% CO_2 for 6–7 days after which the UC tissue was removed and the adherent cells were allowed to expand for an additional week. After approximately 14 days, the adherent cells were harvested by TrypLe Select 1X (Life-Technologies) treatment and re-plated in T175 flasks (BD Falcon) in MSC expansion medium for further expansion.

Before NP loading, immunophenotype analysis and multilineage differentiation potential of cells have been extensively characterized by our group as previously reported (Capelli et al., 2011).

2.3. Cell labeling

At the third passage of culture, UC-MSCs were seeded in 24-well plates on round glass slides at two different concentrations (2000 and 6000 cells/well). After 48 h, UC-MSCs were exposed to positively charged 50 and 200 nm PMMA-NPs with a concentration of $20 * 10^{10}$ and $2.5 * 10^{10}$ NPs/ml respectively. Elapsed 6, 24 and 72 h of NP incubation, the culture medium was removed, UC-MSCs were washed twice with phosphate buffered saline (PBS) and fixed in 4% paraformaldehyde solution for 40 min. Subsequently, Hoechst-33258 dye (Sigma-Aldrich) (2 μg/ml in PBS) was added to fixed cells for 40 min for nuclear staining. At the end of incubation, glass slides were mounted with coverslips with some drops of Fluoromount mounting medium. Confocal microscopy analysis was performed using an Olympus Fluoview microscope BX61 with confocal system FV500, equipped with specific lasers $\lambda exc = 405$ nm, $\lambda exc = 546$ nm, to visualize Hoechst-33258 and RhB respectively. A 3D reconstruction was carried out using Imaris 5.0 (Bitplane) software. Three replicated wells were used for each concentration and time of incubation in all experiments; additional slides without NPs were added as control.

Once determined that UC-MSCs internalize more efficiently PMMA-NPs of 200 nm after 24 h of incubation, a second experiment was executed to assess the most suitable concentration of PMMA-NPs-200 nm. Three different concentrations were tested: $1.25 * 10^{10}$, $2.5 * 10^{10}$ and $10 * 10^{10}$ NPs/ml. The experimental protocol was maintained the same as above described.

2.4. Viability and growth rate

In order to evaluate a possible cytotoxic effect of PMMA-NPs-200 nm, UC-MSCs were seeded directly on the wells and exposed to NPs as described above. After 24 h, they were harvested and cell viability was evaluated both by Trypan blue (Sigma-Aldrich) dye exclusion method and by cytofluorimetric analysis using FACS Canto instrument and FACS Diva software Version 6.1.2.

Cell growth was assessed at different time-points (6, 24, 48, 72 and 120 h) in controls and double-labeled UC-MSCs as previously reported by our group (Cova et al., 2013).

2.5. Animals

Procedures involving animals and their care were conducted in conformity with the institutional guidelines at the IRCCS — Institute for Pharmacological Research "Mario Negri" in compliance with national (Decreto Legge nr 116/92, Gazzetta Ufficiale, supplement 40, February 18, 1992; Circolare nr 8, Gazzetta Ufficiale, July 14, 1994) and international laws and policies (EEC Council Directive 86/609, OJL 358, 1, Dec. 12, 1987; Guide for the Care 1 and Use of Laboratory Animals, U.S. National Research Council, 8th 2 edition, 2011). This specific protocol was approved by the IRCCS-IRFMN Animal Care and Use Committee (IACUC) and then approved by the Italian "Istituto Superiore di Sanità" (code: 17/01 D Appl 3).

Transgenic mice expressing mutant human SOD1 (SOD1G93A), originally obtained from Jackson Laboratories, crossbred with a C57BL/6J mice strain, were chosen as ALS model, while non-transgenic C57BL/6 mice (nTG) were used as controls. For all the experiments, female mice at the age of 14 weeks (corresponding to the pre-onset of clinical signs) were used and maintained in specific pathogen free animal rooms.

A total of seventy female mice were enrolled for the in-vivo studies. They were divided in the following six groups: 1) SOD1G93A mice ICV injected with UC-MSCs (n = 15); 2) nTG mice ICV injected with UC-MSCs (n = 15); 3) nTG mice ICV injected with vehicle (n = 5); 4) SOD1G93A mice IV injected with UC-MSCs (n = 15), 5) nTG mice IV injected with UC-MSCs (n = 15); 6) nTG mice IV treated with vehicle (n = 5).

An additional group of nTg mice (n = 18) was intravenously treated with UC-MSCs. in order to evaluate the fate of UC-MSCs in the early hours after their administration.

2.6. Surgery and transplantation procedures

Labeled UC-MSCs were detached from the culture plates, centrifuged, counted and resuspended in sterile PBS as previously described (Cova et al., 2013).

Fifteen SOD1G93A female mice at age 14 weeks corresponding to the pre-symptomatic stage and the same number of age-matched nTG mice, anesthetized with a 5% isoflurane/oxygen mixture, received 250,000 cells in the anterior horn of the brain lateral ventricles (125,000 for each side) diluted in 8 μl (4 μl for each ventricle). The following stereotaxic coordinates were utilized (Anterior Posterior 0.0 mm from the bregma; Lateral ± 1.0 mm from the bregma; Deepness −3.0 mm from skull surface). Five nTG animals, receiving the same volume of PBS, were used as inner control.

The same number of animals (equally divided among SOD1G93A and nTG mice) systemically received 1,000,000 of UC-MSCs injected in the tail vein. Cells were diluted in 250 μl of PBS to minimize the risk of embolism or thrombi. Five nTG animals, receiving the same volume of PBS, were used as inner control.

Before cell administration, five animals were randomly assigned to the experimental group sacrificed at 1, 7 and 21 days after injection. Another group of 18 mice was intravenously injected with 1,000,000 of UC-MSCs and three mice per group were sacrificed at 1, 3, 6 h, 1 day and 5 days after cell administration to evaluate the distribution of the cells in the whole body.

2.7. In-vivo and ex-vivo imaging

In-vivo whole body fluorescence scanning was performed in living SOD1G93A and nTG mice at 1, 7 and 21 days from UC-MSC administration as previously described (Sitia et al., 2014; Bigini et al., 2014). Thanks to DIR dye, bounded to the PMMA-NPs, we were able to track UC-MSCs with minimal tissue background and high optical contrast. The Explore Optix System (ART Advanced Research Technologies, Montreal, Canada) and a fixed pulsed laser diode as an illumination source was used as already described by our group (Bigini et al., 2014). Excitation was performed with a 735 nm pulsing laser and emission was detected with a 755 nm long pass filter.

Immediately after the mice were sacrificed, ex-vivo optical scan of the isolated kidney, spleen, liver, lung, heart, brain, spinal cord and muscle was carried out to better understand the actual accumulation of signal in each single organ before proceeding with the histological analysis.

2.8. Histological analyses

The brain, spinal cord, lung, kidney, liver, heart, spleen and muscle were rapidly collected, frozen in dry ice and maintained at −80 °C until their use.

Sections with a thickness of 30 μm were obtained after cryostat cutting and observed with a BX81 microscope equipped with an F-view II CDD camera (Olympus).

2.9. Data calculation and statistical analysis

The percentage of cell viability after NP incubation is reported as mean ± S.D. and analyzed by the unpaired Student's t-test. P values ≤0.05 was considered as threshold to establish a statically significant

difference among the groups. One-way analysis of variance (ANOVA), with Bonferroni post-test analysis, was carried out to compare the trend of proliferation of cells with or without double labeling with PMMA-NPs and Hoechst-33258.

All statistical analyses were done using the GraphPad Prism version 4.00 for Windows (Graph-Pad Software, San Diego, CA, USA).

3. Results and discussion

3.1. In-vitro results

The first requirement in experiments of cell labeling is the fast and efficient internalization of tracers in the target. To verify it, the rate of

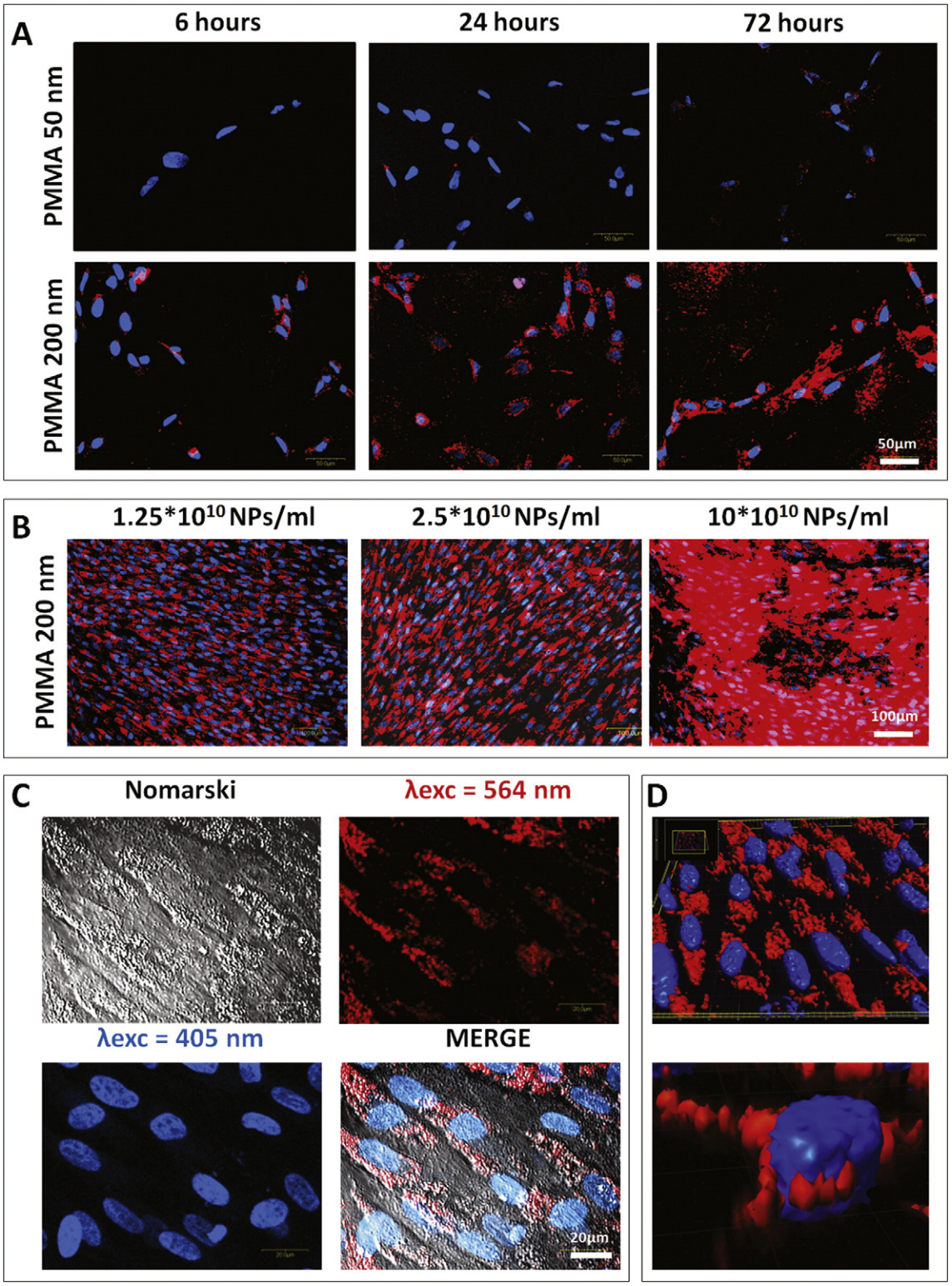

Fig. 1. Representative confocal microscopy images showing A) UC-MSCs incubated for 6, 24 and 72 h with 50 nm (upper panel) and 200 nm (lower panel) large PMMA-NPs; B) UC-MSCs incubated for 24 h with three different concentrations of 200 nm PMMA-NPs. The red signal is associated with NPs; the blue staining is associated with the nuclear dye Hoechst-33258. C) UC-MSCs incubated with PMMA-NPs after 24 h. D) 3D reconstruction of treated cells is reported at low and high magnifications.

internalization and the cellular localization of NPs were evaluated incubating UC-MSCs 6, 24 and 72 h with PMMA-NPs. Hoechst-33258 was used to label cell nuclei. NPs of two different sizes were tested (50 and 200 nm large NPs) in order to establish the more efficient labeling agent. Representative images showing the distribution of both 50 and 200 nm large NPs at the three different time points are reported in Fig. 1A. As expected, the Hoechst-33258 nuclear labeling (visualized in blue) was already at the maximum levels at the first time point of analysis and remained stable for the whole observation. In contrast, NP internalization was a slower process that progressively increased over time. In particular, the staining for 50 nm large PMMA-NPs was almost undetectable up until one day of incubation and the interaction for three days produced a very weak signal (Fig. 1A, upper panels). On the contrary, cell incubated with 200 nm large PMMA-NPs resulted in a much higher fluorescent signal. At 6 h, a strong NP signal was already detectable in incubated cells and it was mainly confined to the peripheral region of the cytoplasm. At later time points, NPs progressively internalized and uniformly occupied the whole cytoplasm (Fig. 1A lower panels). Recent studies, performed by our group, have shown that the NP size did not greatly influence the number of NPs internalized in cells (Sitia et al., 2014; Ferrari et al., 2014). This evidence strongly suggests that the difference among the two types of NPs is mainly due to the higher amount of RhB for each single NP in 200 nm large NPs. In addition, we found that larger NPs are more efficiently enwrapped in inert endosomes and stay for a longer time in host cells without any relevant perturbation. For these reasons, we decided to carry on the experiments using 200 nm large PMMA-NPs and stopping the incubation at the 24th hour (where the cellular signal associated with RhB was evident for almost all cells and the background was nearly absent).

Once fixed the size of NPs and the length of incubation to be used, a dose response experiment was carried out to verify the most appropriate NP concentration. As depicted in Fig. 1B, already with the lower concentration [$1.25 * 10^{10}$ NPs/ml] a uniform and strong labeling was induced. Higher concentrations did not increase either the percentage of labeled cells or the specific signal intensity. On the other hand, a strong non-specific NP-related signal was observed at the highest dose.

The optimization of the procedure of stem cell labeling was necessary to define a protocol for in-vivo and ex-vivo tracking. We found an efficient labeling of all cells 24 h after NP incubation. Opposite the prolonged incubation did not increase intracellular staining but led to membrane not specific staining. Positively charged polymeric NPs rapidly undergo to an electrostatic attraction to the outer portion of the cell membrane, this interaction leads to vesicle formation and consequent cytoplasmic endocytosis of NPs segregated in this vesicles (Sahay et al., 2010). This process occurs in the first hours of incubation and progressively decreased probably for the lack of the vesicle availability. This biological limit may therefore cause the accumulation of NPs to the external surface without an efficient endocytosis and their consequent risk of a rapid leakage in the biological fluids after their injection (Duan and Li, 2013; Shah et al., 2012). Freely circulating NPs in plasma rapidly interact with immunocompetent cells, reticulocytes, Kupffer cells in the liver and splenic macrophages. For this reason to furthermore reduce the presence of false negative (due to the staining of host cells that have uptake free circulating NPs) we also included the nuclear marker Hoechst-33258 as previously reported (Bigini et al., 2012; Cova et al., 2013). However, this procedure should be always guaranteed by an earlier control of the effective cellular internalization of NPs at least until the time of inoculation.

A more detailed representation of tracer localization in UC-MSCs is shown in Fig. 1C where the same field-of-view is depicted in four different manners, 24 h after incubation. In the left-up image the shape of plated cells using the interferential contrast (Nomarski) can be observed; in the left-bottom image the signal from the channel associated with Hoechst-33258 is shown revealing the segregation of such marker in the nuclear region as expected. Most importantly, the merge image revealed that the signal associated with NPs (red) does not co-localize with blue nuclear staining and it is confined to the cell surface. A representative 3D scanning of double labeled UC-MSCs is shown in Fig. 1D. In the upper panel, a low magnified picture enhances the contrast and the separation among the two tracers; the lower panel is of interest to unmask the clear contiguity between NPs and Hoechst-33258 without any superimposition. This is in line with our recent results showing that PMMA-NPs rapidly diffused toward the cytoplasm mainly localizing to the perinuclear region (colocalization with Golgi apparatus and endoplasmic reticulum has been demonstrated) (Sitia et al., 2014).

The possible cellular perturbation of size (FSC) and granularity (SSC) after NP incubation was measured by FACS analysis. Fig. 2A shows the presence of a morphologically distinct cell population (P1, red) in cells exposed to NPs. The cluster of cells included in P2 (green) showed size and granularity typical of these mesenchymal cells. The P1 group

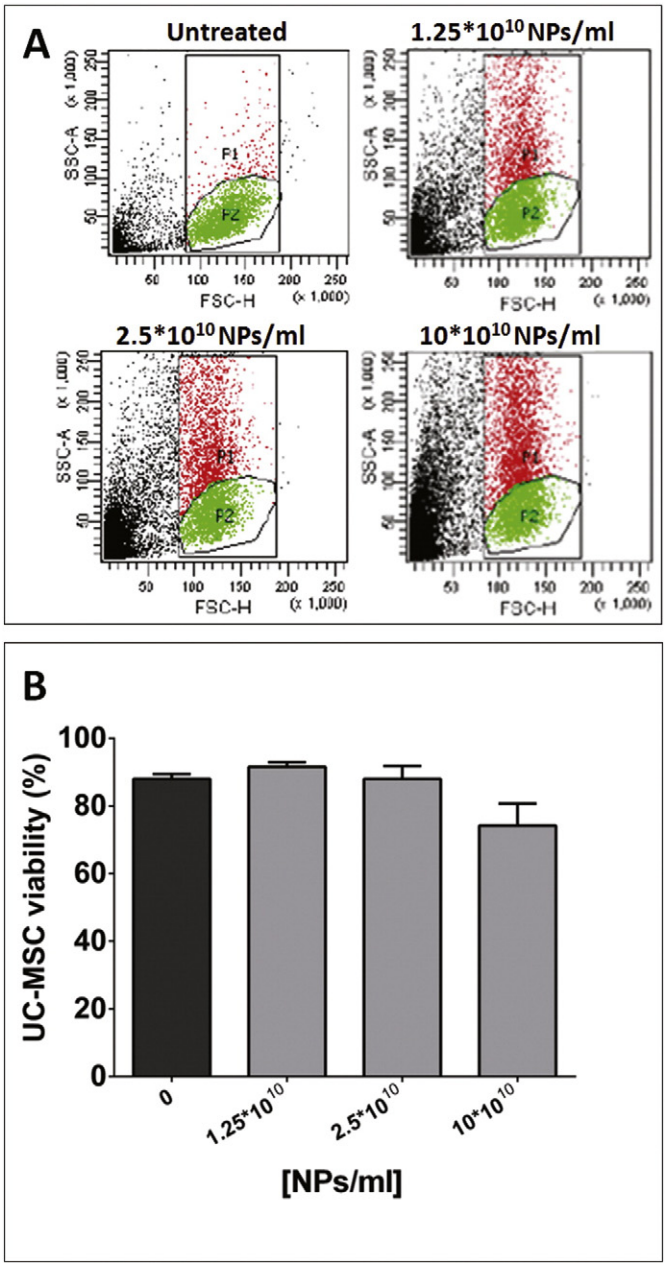

Fig. 2. A) Analysis of size (FSC) and granularity (SSC) of UC-MSCs before and after the incubation with three different concentrations of PMMA-NPs. B) Effect of different concentration of 200 nm PMMA-NPs on UC-MSC. Cell viability was determined by Trypan blue dye exclusion method. Data are expressed mean ± S.D. and analyzed by the unpaired Student's t-test.

(red) was characterized by a rise in the levels of Side Scatter. This likely indicated changes of cellular complexity due to a partial change in the internal morphology and in the surface roughness of the cell after vesicles-dependent NP internalization (Sitia et al., 2014). FACS analysis confirmed the previous results shown in Fig. 1B. In addition, no significant difference on cell survival was detectable 24 h after NP incubation for each concentration used, compared to untreated cells (Fig. 2B). The analysis of cell proliferation revealed a similar trend of growth rate for both unlabeled and double labeled cells. Both experimental groups showed a first phase (0 to 24 h) of mild increase of rate. At the following time, until the 72nd hour, the slope of the growth was higher for both groups. From the 72nd to the 120th hours the growth rate slightly decreased. However this reduction in growth rate at the latter time-point could be likely due to the confluence on the plate. Neither the analysis of variance nor the student t-test at each single time-point revealed difference among the two experimental groups. This result further suggests that the labeling did not markedly alter the cell physiology.

All these results, in agreement with previous studies (Cova et al., 2013; Srivastava and Bulte, 2014), allowed us to exploit this safe and efficient procedure of labeling to follow the fate of transplanted UC-MSCs in mice.

3.2. In-vivo results

Based on the in-vitro analysis, the concentration of $1.25 * 10^{10}$ NPs/ml of PMMA-NPs-200 nm was chosen for the in-vivo studies. Representative images of fluorescence distribution by in-vivo Optical Imaging in both SOD1G93A and nTG mice are reported in Fig. 3A. Due to the high level of autofluorescence of tissues in the visible wavelengths (associated to RhB), the presence of the DIR dye ($\lambda = 735$ nm) allowed us to improve the signal/background ratio thus optimizing the quality and the reliability of in-vivo imaging observations. The laser power was finely tuned in order to avoid as much as possible the non-specific signal of the tissue using mice treated with vehicle alone (see Fig. 3A left panel). One day after IV administration of UC-MSCs a strong signal was spread in the thoraco-abdominal area. In particular, an intense signal was found close to the region corresponding to the lungs (top) and liver (bottom). Seven days after cell injection, a similar pattern of signal distribution, even if of lower fluorescence intensity (FLI), was observed. A drastic reduction of FLI was instead observed three weeks after UC-MSC administration. The overall FLI pattern registered was nearly overlapping among the five mice tested for each experimental group, indicating good homogeneity in the stem cell localization. The pattern of distribution and FLI was similar between SOD1G93A and nTG mice.

To better assess if the signal was actually independent on the autofluorescence, a quantitative analysis of the specific signal was carried out through the evaluation of the Temporal Point-Spread Function (TPSF). This parameter is unequivocally correlated to the different signals (e.g. specific signal from tissue autofluorescence) discriminating them on the base of their amplitude and the slope of the curves. Representative TPSF profiles from a well-defined point of the abdominal region from a control mouse (green) and three SOD1G93A mice sacrificed 1 (yellow), 7 (red) and 21 (blue) days after UC-MSCs injection are shown in Fig. 3B. The strong difference between the curves of the mice at 1 and 7 days and the vehicle further confirms that the fluorescent signal observed in the scanning area is correlated to the presence of DIR-loaded NPs. On the other hand, this difference strongly decreased in animals sacrificed 21 days after transplantation.

Ex-vivo Optical Imaging was then carried out after the mice sacrifice to determine the organ specificity of the signal. The FLI measurements for lung, spleen and liver are shown in Fig. 3C. A progressive decay of FLI was observed for both experimental groups. No signal was found in kidneys, heart, brain, spinal cord and muscle (data not shown). These results are consistent with the anatomical distribution of the signal observed in living mice and confirm the reliability of this system of in-vivo stem cell tracking. Two main advantages should be underlined in comparison to other imaging technique, such as MRI to detect cells incubated with SPIOn or ultrasounds coupled photoacoustic analysis to reveal cells incubated with gold NPs (Jokerst et al., 2012; Bull et al., 2014). The first is that fluorescent polymeric NPs can be directly tracked in organs by visualizing their fluorescence in histological sections in preclinical studies to correlate easily and rapidly in-vivo and ex-vivo analyses. The second, and most important, is the possibility of easily modulating their biodegradability and avoids risks of NP bio-accumulation in case of repeated stem cell administrations. This will be of fundamental relevance in future translational studies that might open the way toward a clinical application of this approach in different clinical fields.

The labeling of human adult mesenchymal stem cells (hMSCs) with near-infrared dye has been recently used for their tacking after intranasal administration in rats (Bossolasco et al., 2012). In that study, the signal related to hMSCs was only detectable few minutes after application to completely disappear into the scanned area (brain, head and neck) within 1 h. This rapid clearance may be due to the efficient

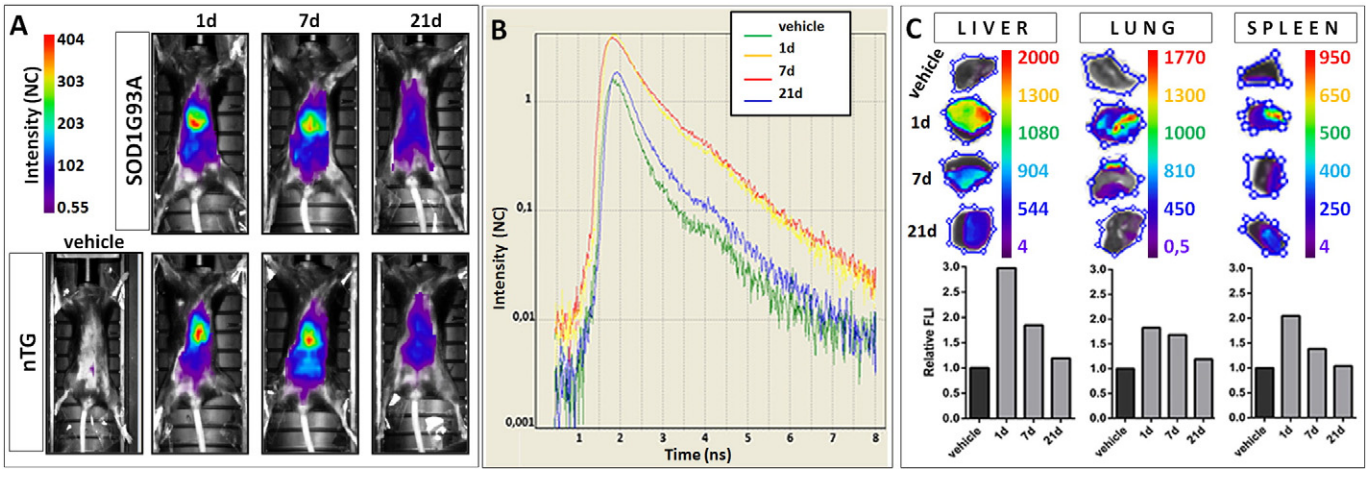

Fig. 3. A) In vivo near-infrared fluorescent scans of SOD1G93A (upper panel) and nTG mice (lover panel) intravenously treated with labeled UC-MSCs. Representative images were acquired before (vehicle) administration, and at different time points (1, 7 and 21 days) after stem cell administration. The fluorescence signal intensity, measured as normalized photon counts (NC), is shown as a pseudo-color scale bar. B) Temporal point-spread function (TPSF) acquired from the untreated mouse to the mice sacrificed 1, 7 and 21 days after UC-MSCs injection. Both SOD1G93A and nTG mice show the same curve. C) Ex vivo biodistribution and accumulation of UC-MSCs in the liver, lung and spleen before and after injection (1, 7 and 21 days). At each time point, the signal derived from the excised organs was quantified and expressed as relative fluorescent intensity (FLI). The value of the vehicle treated animals was normalized to 1.

metabolism and the tropism to filter organs, in particular the lungs, after systemic administration of mesenchymal cells or related to a rapid leakage through plasmatic membrane and consequent biological elution (Nystedt et al., 2013; Vaegler et al., 2014; Tenuta et al., 2011; Zoja et al., 2012).

Histological analyses were carried out to confirm the association between fluorescent signal and the actual presence of UC-MSCs with a higher degree of resolution. Representative images of the lungs (left column), spleen (middle column) and liver (right column) from both SOD1G93A (upper panels) and nTG mice (lower panels) are shown one day after UC-MSC transplantation in Fig. 4A. Seven and 21 days after IV administration no specific signal was detectable from histological sections in both nTG and SOD1G93A mice (data not shown). In red and in blue the signal of NPs and the nuclear dye Hoechst-33258 can be observed respectively. No relevant difference in terms of NP distribution was observed within the two experimental groups, in all analyzed organs.

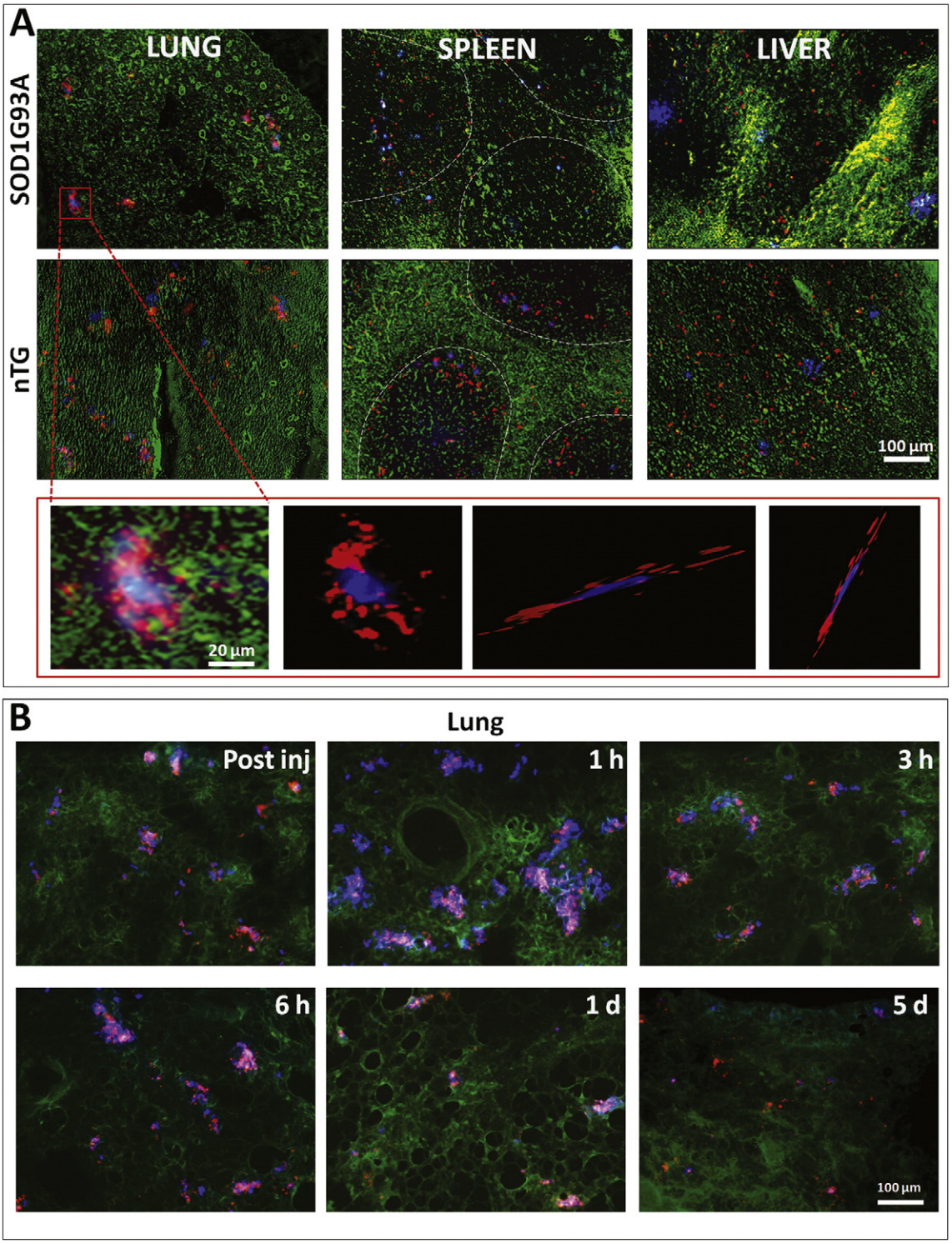

Fig. 4. A) Histological sections of lung, spleen and liver from SOD1G93A (upper panel) and nTG (lower panel) mice sacrificed 1 day after UC-MSCs injection. B) Histological sections of lung parenchyma derived from mice sacrificed immediately, 1 h, 3 h, 6 h, 1, and 5 days after UC-MSCs injection. The green staining is related to the autofluorescence of tissues. The red staining is associated with PMMA-NPs and the blue spot is referred to UC-MSC nuclei.

In the lungs of both nTG and SOD1G93A mice numerous cells were found uniformly distributed throughout all the parenchyma. The injected cells maintained their perfect integrity as demonstrated by the fact that the red (cytoplasm) and the blue (nuclei) signals remain contiguous.

Several studies have shown that the majority of IV-administered cells, especially MSCs, are trapped within the lungs at least during the acute phase after administration (Fischer et al., 2009; Schrepfer et al., 2007). Different key factors may influence this entrapment, such as the kind, the size and the adhesion capacity of the injected cells. The mean diameter of adult mouse pulmonary capillaries is approximately 15 μm, and larger cells are consequently trapped within the lungs. In addition, it is reported that UC-MSCs express high levels of α4 integrin, α6 integrin and fibronectin: this cell surface profile contributes to the adhesion on the alveolar endothelium (Ruster et al., 2006).

In our experimental condition, UC-MSCs almost exclusively accumulated in the lungs, and gradually moved to the reticuloendothelial organs. In both spleens, where the signals are confined in the lymphoid follicles, (Fig. 4A, middle panels) and liver (Fig. 4A, right panels), the NP-related signal (red) was clearly separated from the nuclear dye Hoechst-33258. Therefore, it is clear that a very high percentage of intravenously injected UC-MSCs are rapidly and efficiently captured by the lungs before reaching the filter organs (spleen and liver) for their metabolism and clearance. In fact, while in the lung parenchyma the cells were still present one day after the treatment and their integrity was confirmed histopathologically by the contiguity of the two markers (red for NPs and blue for nuclei), in the spleen and in the liver there were only cellular debris and free nanoparticles (Fig. 4A). Even in the first 6 h when the labeled UC-MSCs were clearly visible in the lung (Fig. 4B), no cells were noticed in the spleen and liver (data not showed).

As regards other organs, no cells were observed in kidney sections in both experimental groups and for each time-points considered, in line with the lack of signal found in ex-vivo Optical Imaging analysis. Moreover, no specific UC-MSC related signal was detected in brain cortex, brainstem, spinal cord and muscles of SOD1G93A mice that, in the present study, were followed from the 14th week to the 17th week of life corresponding to the early phase of the disease progression (Doble and Kennel, 2000). The same result was found for age-matched nTG mice. The observation of numerous sections from the different organs allowed us to make a semiquantitative analysis of the localization, accumulation and clearance in different organs of intravenously treated mice (Fig. 5B).

The main results emerging from this results are that: 1) intravenously injected UC-MSCs were well tolerated by both healthy and neurologically affected mice; 2) UC-MSCs mainly accumulated in the lungs and rapidly faded away without any problem of accumulation; 3) the pathological state neither induced a selective migration of UC-MSC toward affected areas nor altered their half-life; 4) the triple systems of tracking exploiting three different optical profiles is resulted particularly performing and reliable for a whole body screening.

A relevant aspect of using labeling agents in cell-based therapy regards their safety. In fact, both potential health risks for final hosts and possible effects on the cells due to their labeling, should be avoided at preclinical and clinical level. SPIOn has been widely used for stem cell tracking and several published studies showed their reliability in terms of low toxicity profiles. For these reasons, they have been considered to be inert and biocompatible for a long time (Bull et al., 2014).

However, an even more growing body of evidence is showing iron accumulation could impair cell viability by damaging cell membranes, misfolding proteins, inducing mitochondrial function impairment, DNA strand breaks, ROS generation and cytoskeleton alterations (Mahmoudi et al., 2012). In this context, it has been recently demonstrated that SPIOn loading inhibited cell growth, proliferation rates and motility (Diana et al., 2013). In spite of these pitfalls, MRI still remains one of the most suitable techniques for in-vivo longitudinal tracking of administered stem cells in mice due to its high spatial resolution and deep tissue penetrance.

However, alternative methods, such as the use of Optical Imaging technique, coupled to fluorescent NPs, may be preferred for its higher sensitivity, the possibility to easily generate a quantitative correlation

A

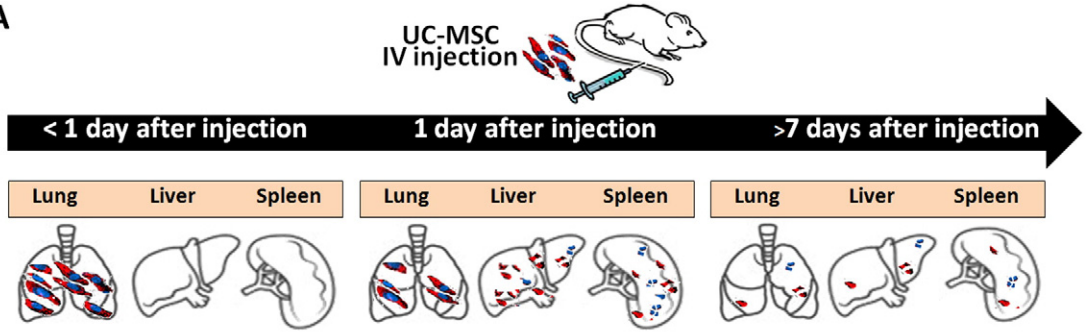

B

IV ADMINISTRATION		BRAIN	SPINAL CORD	LUNG	LIVER	SPLEEN	KIDNEY	MUSCLE
< 1 DAY	SOD1G93A	-	-	++++	-	-	-	-
	nTG	-	-	++++	-	-	-	-
1 DAY	SOD1G93A	-	-	++	+/-	+/-	-	-
	nTG	-	-	++	+/-	+/-	-	-
> 7 DAYS	SOD1G93A	-	-	+/-	-	-	-	-
	nTG	-	-	+/-	-	-	-	-

Fig. 5. A) Schematic representation of UC-MSC biodistribution after intravenous injection. B) Scores associated with cell distribution after intravenous administration of UC-MSCs. The analysis was carried out in different organs, animals and time points. – none, +/− very few (rare), + few, ++ relevant, ++++ high.

between signal and labeling agent concentration, the detection of signal in regions where endogenous iron is already relevant, (such as in the spleen where the visualization of SPIOn labeled cells is impaired) and, last but not least, the rapid analysis of the whole body, should not be neglected (Sutton et al., 2008). The lack of relevant side-effects and the survival of all mice confirmed the high degree of biocompatibility of PMMA-NPs for stem cell tracking experiments.

We observed that once injected in the bloodstream, the cells mainly localized in lung parenchyma and to a lesser extent in the spleen and liver. However, the clearance of the cells was rapid and, seven days after the treatment, their number was found drastically reduced and no accumulation was registered.

Even if intravenous approach would be ideal, given easy access, questions have been raised due to the poor survival of grafted cells after pulmonary first-pass effect. This phenomenon may preclude the efficacy of the stem cells in a chronic disease such is the ALS.

To overcome this limit, different strategies could be applied. Several groups are developing biocompatible scaffolds loaded with stem cells, based on local controlled delivery and introduced in animals using minimally invasive surgical procedures (Wong et al., 2014). Moreover, other recent studies reported the possibility to subcutaneously inject stem cell encapsulated in Alginate (Zanotti et al., 2013). This procedure prevents possible risks related to cell transplantation (tumor growth, graft rejection or uncontrolled differentiation) and permits a precise dosage released over time. These systems could provide cell local release able to reduce systemic side effects or excessive cell elution through the body, concentrating the treatment efficacy in the pathological areas to improve stem cell therapy of neurological disorders.

Another approach could be the multiple dosing of stem cells (weekly administrations) already evaluated in different models of neurodegenerative disorders, including ALS (Garbuzova-Davis et al., 2012).

Multiple transplantations could provide long-term therapeutic effects than single transplantation, this approach can be used in future clinical studies. In the last decade the effect of human cord blood mononuclear cells (HuCB-MNCs) transplantation has been carried out in different mouse models, with different schedule treatments and by

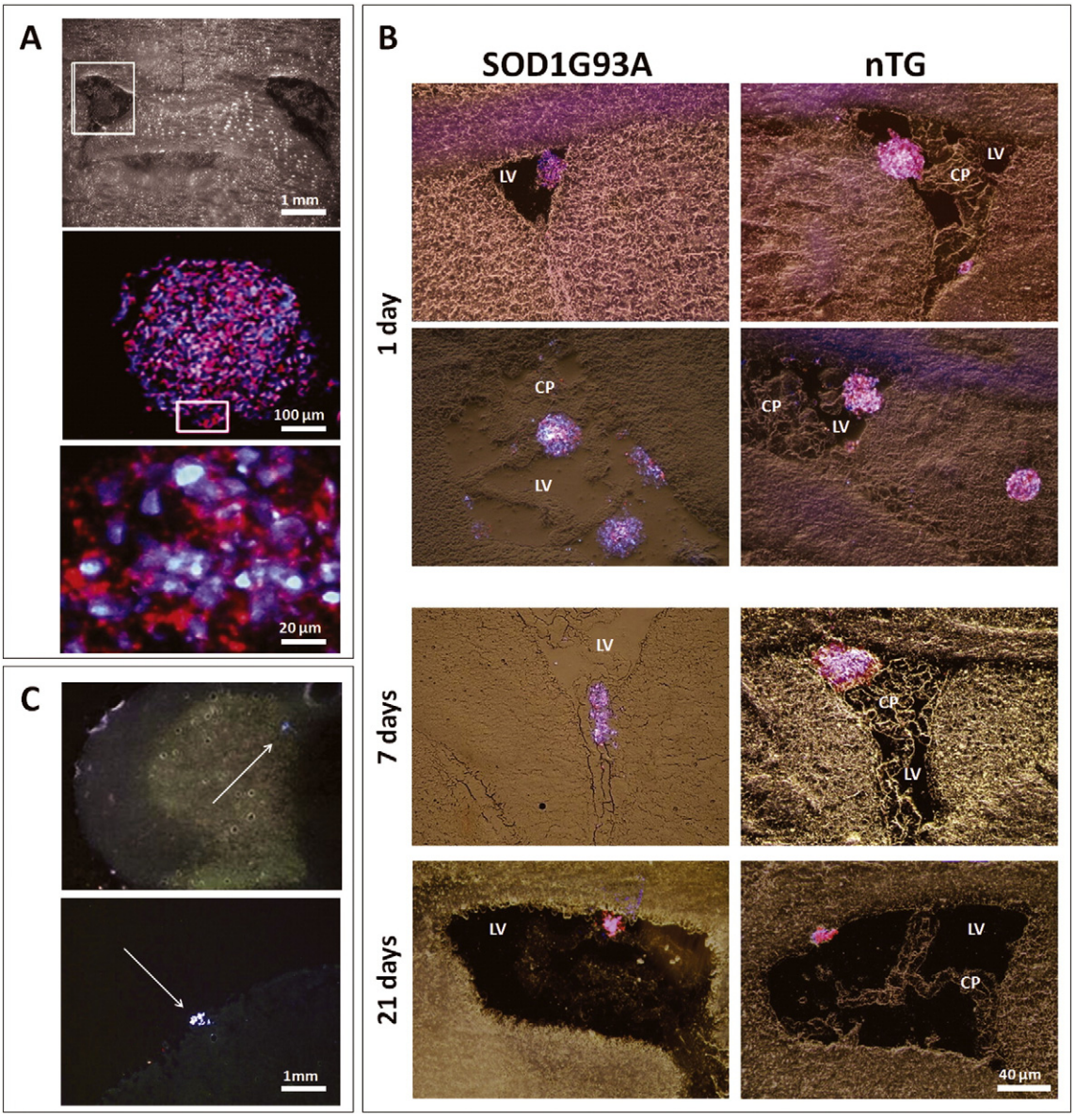

Fig. 6. A) Anatomical detail of the injection site of UC-MSCs during intracerebroventricular transplantation (upper picture); high magnification confocal images referring to the UC-MSC aggregates found into the lateral ventricles of treated mice (lower pictures). B) Representative images showing the localization of double labeled UC-MSCs in the brain of SOD1G93A and nTG mice sacrificed after 1, 7 and 21 days from cell administration. (LV = Lateral ventricle, CP = Choroid plexus) C) Sporadic clusters of UC-MSCs found in cervical spinal cord sections exclusively 1 day after SOD1G93A mice were sacrificed.

different ways of administrations (Chen and Ende, 2000; Garbuzova-Davis et al., 2003; Knippenberg et al., 2012; Souayah et al., 2012). Quite interestingly, the transplantation of HuCB-MNCs in the cerebral lateral ventricles or in the bloodstream in transgenic SOD1G93A mice showed a similar pattern of clinical and neuropathological benefits mainly characterized by an overall delay in symptoms progression, anti-inflammatory activity and increased lifespan (Garbuzova-Davis et al., 2008; Bigini et al., 2011; Garbuzova-Davis et al., 2012). This result further confirmed that neuroprotective effect may be ascribed by a wide range of cells, sharing the ability to respond to stress conditions by expressing and releasing therapeutic factors.

In this context, to make a comparative evaluation on the behavior of UC-MSCs in murine model of ALS, an extensive investigation on the distribution of UC-MSCs after ICV transplantation has been undertaken in this study at the same time-points reported for IV analysis but using a lower number of cells. Fig. 6A shows UC-MSCs (middle and lower panels) 1 day after lateral brain ventricle administration (upper panel) in a SOD1G93A mouse. A strong signal associated with Hoechst-33258 and RhB clearly indicates the presence of a cluster of UC-MSCs arranged to form large spherical aggregates, inside the lateral ventricle. Higher magnified picture (bottom) furthermore confirms the segregation between the two markers as previously shown by in-vitro analysis (Fig. 1).

A representative pattern of longitudinal UC-MSC distribution in SOD1G93A (left column) and nTG mice (right column) is shown in Fig. 6B. One day after transplantation, injected cells remain in the site of administration, localizing in the lateral ventricles and slightly in the other more caudal ventricular structures. One and three weeks after UC-MSC injection, the size and the number of events forming these cell clusters markedly decreased, even if each single remaining cell was still detectable. No cell has been detected into the brain parenchyma, while observation of spinal cord slices revealed only isolated positive cells localized both in the parenchyma and in the external surface, probably associated with meningeal layers (Fig. 6C).

In agreement with our previous studies (Canzi et al., 2012; Bigini et al., 2011), we observed a very limited number of events inside the spinal cord. This phenomenon may be associated with anatomical and structural limitations that prevent the migration of cell aggregates in this area. In animals sacrificed 21 days after implantation, there is still a mild signal related to the cells only associated with the walls of the ventricles and the choroid plexus, significantly reduced compared to the other two timelines. No substantial differences were observed between the experimental groups (nTG and SOD1G93A mice). A summary of the results obtained by the observation of a large number of sections is shown in Fig. 7.

In conclusion, tracking these cells with biocompatible, well tolerated and stable NPs represents a great advantage during in-vitro, in-vivo and ex-vivo analyses. In particular, in-vivo Optical Imaging after UC-MSC intravenous injection has showed very satisfactory results. This technique provides non-invasive, localized and quantitative information regarding biodistribution, accumulation and clearance. It allows follow-up studies to be carried out within the same experimental subject contributing in reducing the number of animals. Even if Optical Imaging showed lower degree of spatial resolution in living tissues when compared with other types of imaging modalities such as MRI, it is more sensible and suitable for each kind of tissue.

The route of administration may surely influence the efficacy of stem cell therapy. IV injection differs from ICV injection with respect to cellular distribution and number of cells still viable overtime. If after systemic injection pulmonary sequestration may cause cell death within 1 day after treatment, probably the most appropriate way of administration to evaluate UC-MSC therapeutic effect is the application to the cerebrospinal fluid.

Acknowledgments

The authors are grateful to “Associazione IBIS” and “Associazione Amici del Mario Negri” for their support in this research.

A

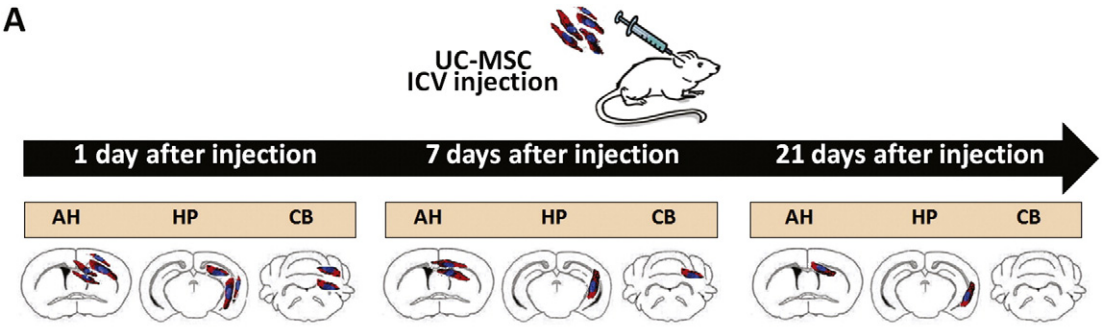

B

ICV ADMINISTRATION		LATERAL VENTRICLES (Anterior Horns AH)	LATERAL VENTRICLES (Hippocampus HP)	BRAIN VESSEL (Cerebellum CB)	SPINAL CORD	LUNG	LIVER	MUSCLE
1 DAY	SOD1G93A	+++	+++	++	+/-	-	-	-
	nTG	+++	+++	++	-	-	-	-
7 DAYS	SOD1G93A	++	+	+	+	-	-	-
	nTG	++	++	+	-	-	-	-
21 DAYS	SOD1G93A	+	+	-	+/-	-	-	-
	nTG	+	-	-	-	-	-	-

Fig. 7. A) Schematic representation of UC-MSC biodistribution after intracerebroventricular injection. (AH = Anterior Horns, HP = Hippocampus, CB = Cerebellum) B) Scores associated with cell distribution after intracerebroventricular administration of UC-MSCs. The analysis was carried out in different organs, animals and time points. – none, +/− very few (rare), + few, ++ relevant, +++ high.

References

Al-Chalabi, A., Hardiman, O., 2013. The epidemiology of ALS: a conspiracy of genes, environment and time. Nat. Rev. Neurol. 9, 617–628.

Bigini, P., Veglianese, P., Andriolo, G., Cova, L., Grignaschi, G., Caron, I., Daleno, C., Barbera, S., Ottolina, A., Calzarossa, C., Lazzari, L., Mennini, T., Bendotti, C., Silani, V., 2011. Intracerebroventricular administration of human umbilical cord blood cells delays disease progression in two murine models of motor neuron degeneration. Rejuvenation Res. 14, 623–639.

Bigini, P., Diana, V., Barbera, S., Fumagalli, E., Micotti, E., Sitia, L., Paladini, A., Bisighini, C., De Grada, L., Coloca, L., Colombo, L., Manca, P., Bossolasco, P., Malvestiti, F., Fiordaliso, F., Forloni, G., Morbidelli, M., Salmona, M., Giardino, D., Mennini, T., Moscatelli, D., Silani, V., Cova, L., 2012. Longitudinal tracking of human fetal cells labeled with super paramagnetic iron oxide nanoparticles in the brain of mice with motor neuron disease. PLoS One 7, e32326.

Bigini, P., Previdi, S., Casarin, E., Silvestri, D., Violatto, M.B., Facchin, S., Sitia, L., Rosato, A., Zuccolotto, G., Realdon, N., Fiordaliso, F., Salmona, M., Morpurgo, M., 2014. In vivo fate of avidin-nucleic acid nanoassemblies as multifunctional diagnostic tools. ACS Nano 8, 175–187.

Bjorklund, A., Lindvall, O., 2000. Cell replacement therapies for central nervous system disorders. Nat. Neurosci. 3, 537–544.

Bossolasco, P., Cova, L., Levandis, G., Diana, V., Cerri, S., Lambertenghi Deliliers, G., Polli, E., Silani, V., Blandini, F., Armentero, M.T., 2012. Noninvasive near-infrared live imaging of human adult mesenchymal stem cells transplanted in a rodent model of Parkinson's disease. Int. J. Nanomedicine 7, 435–447.

Bull, E., Madani, S.Y., Sheth, R., Seifalian, A., Green, M., Seifalian, A.M., 2014. Stem cell tracking using iron oxide nanoparticles. Int. J. Nanomedicine 9, 1641–1653.

Calero, M., Gutierrez, L., Salas, G., Luengo, Y., Lazaro, A., Acedo, P., Morales, M.P., Miranda, R., Villanueva, A., 2014. Efficient and safe internalization of magnetic iron oxide nanoparticles: two fundamental requirements for biomedical applications. Nanomedicine 10, 733–743.

Canzi, L., Castellaneta, V., Navone, S., Nava, S., Dossena, M., Zucca, I., Mennini, T., Bigini, P., Parati, E.A., 2012. Human skeletal muscle stem cell antiinflammatory activity ameliorates clinical outcome in amyotrophic lateral sclerosis models. Mol. Med. 18, 401–411.

Capelli, C., Gotti, E., Morigi, M., Rota, C., Weng, L., Dazzi, F., Spinelli, O., Cazzaniga, G., Trezzi, R., Gianatti, A., Rambaldi, A., Golay, J., Introna, M., 2011. Minimally manipulated whole human umbilical cord is a rich source of clinical-grade human mesenchymal stromal cells expanded in human platelet lysate. Cytotherapy 13, 786–801.

Cheah, B.C., Vucic, S., Krishnan, A.V., Kiernan, M.C., 2010. Riluzole, neuroprotection and amyotrophic lateral sclerosis. Curr. Med. Chem. 17, 1199–1942.

Chen, R., Ende, N., 2000. The potential for the use of mononuclear cells from human umbilical cord blood in the treatment of amyotrophic lateral sclerosis in SOD1 mice. J. Med. 31, 21–30.

Corti, S., Locatelli, F., Donadoni, C., Guglieri, M., Papadimitriou, D., Strazzer, S., Del Bo, R., Comi, G.P., 2004. Wild-type bone marrow cells ameliorate the phenotype of SOD1-G93A ALS mice and contribute to CNS, heart and skeletal muscle tissues. Brain 127, 2518–2532.

Cova, L., Bigini, P., Diana, V., Sitia, L., Ferrari, R., Pesce, R.M., Khalaf, R., Bossolasco, P., Ubezio, P., Lupi, M., Tortarolo, M., Colombo, L., Giardino, D., Silani, V., Morbidelli, M., Salmona, M., Moscatelli, D., 2013. Biocompatible fluorescent nanoparticles for in vivo stem cell tracking. Nanotechnology 24, 245603.

Diana, V., Bossolasco, P., Moscatelli, D., Silani, V., Cova, L., 2013. Dose dependent side effect of superparamagnetic iron oxide nanoparticle labeling on cell motility in two fetal stem cell populations. PLoS One 8, e78435.

Doble, A., Kennel, P., 2000. Animal models of amyotrophic lateral sclerosis. Amyotroph. Lateral Scler. Other Motor. Neuron Disord. 1, 301–312.

Duan, X., Li, Y., 2013. Physicochemical characteristics of nanoparticles affect circulation, biodistribution, cellular internalization, and trafficking. Small 9, 1521–1532.

Ferrari, R., Lupi, M., Falcetta, F., Bigini, P., Paolella, K., Fiordaliso, F., Bisighini, C., Salmona, M., D'Incalci, M., Morbidelli, M., 2014. Integrated multiplatform method for in vitro quantitative assessment of cellular uptake for fluorescent polymer nanoparticles. Nanotechnology 25, 045102.

Fischer, U.M., Harting, M.T., Jimenez, F., Monzon-Posadas, W.O., Xue, H., Savitz, S.I., Laine, G.A., Cox Jr., C.S., 2009. Pulmonary passage is a major obstacle for intravenous stem cell delivery: the pulmonary first-pass effect. Stem Cells Dev. 18, 683–692.

Garbuzova-Davis, S., Willing, A.E., Zigova, T., Saporta, S., Justen, E.B., Lane, J.C., Hudson, J.E., Chen, N., Davis, C.D., Sanberg, P.R., 2003. Intravenous administration of human umbilical cord blood cells in a mouse model of amyotrophic lateral sclerosis: distribution, migration, and differentiation. J. Hematother. Stem Cell Res. 12, 255–270.

Garbuzova-Davis, S., Sanberg, C.D., Kuzmin-Nichols, N., Willing, A.E., Gemma, C., Bickford, P.C., Miller, C., Rossi, R., Sanberg, P.R., 2008. Human umbilical cord blood treatment in a mouse model of ALS: optimization of cell dose. PLoS One 3, e2494.

Garbuzova-Davis, S., Rodrigues, M.C., Mirtyl, S., Turner, S., Mitha, S., Sodhi, J., Suthakaran, S., Eve, D.J., Sanberg, C.D., Kuzmin-Nichols, N., Sanberg, P.R., 2012. Multiple intravenous administrations of human umbilical cord blood cells benefit in a mouse model of ALS. PLoS One 7, e31254.

Gordon, P.H., 2013. Amyotrophic lateral sclerosis: an update for 2013 clinical features, pathophysiology, management and therapeutic trials. Aging Dis. 4, 295–310.

Griffin, M.D., Elliman, S.J., Cahill, E., English, K., Ceredig, R., Ritter, T., 2013. Concise review: adult mesenchymal stromal cell therapy for inflammatory diseases: how well are we joining the dots? Stem Cells 31, 2033–2041.

Harms, M.B., Baloh, R.H., 2013. Clinical neurogenetics: amyotrophic lateral sclerosis. Neurol. Clin. 31, 929–950.

Jokerst, J.V., Thangaraj, M., Kempen, P.J., Sinclair, R., Gambhir, S.S., 2012. Photoacoustic imaging of mesenchymal stem cells in living mice via silica-coated gold nanorods. ACS Nano 6, 5920–5930.

Knippenberg, S., Thau, N., Schwabe, K., Dengler, R., Schambach, A., Hass, R., Petri, S., 2012. Intraspinal injection of human umbilical cord blood-derived cells is neuroprotective in a transgenic mouse model of amyotrophic lateral sclerosis. Neurodegener. Dis. 9, 107–120.

Li, L., Jiang, W., Luo, K., Song, H., Lan, F., Wu, Y., Gu, Z., 2013. Superparamagnetic iron oxide nanoparticles as MRI contrast agents for non-invasive stem cell labeling and tracking. Theranostics 3, 595–615.

Lindvall, O., Kokaia, Z., 2006. Stem cells for the treatment of neurological disorders. Nature 441, 1094–1096.

Mahmoudi, M., Hofmann, H., Rothen-Rutishauser, B., Petri-Fink, A., 2012. Assessing the in vitro and in vivo toxicity of superparamagnetic iron oxide nanoparticles. Chem. Rev. 112, 2323–2338.

Mitrecic, D., Nicaise, C., Gajovic, S., Pochet, R., 2010. Distribution, differentiation, and survival of intravenously administered neural stem cells in a rat model of amyotrophic lateral sclerosis. Cell Transplant. 19, 537–548.

Musaro, A., 2013. Understanding ALS: new therapeutic approaches. FEBS J. 280, 4315–4322.

Nystedt, J., Anderson, H., Tikkanen, J., Pietila, M., Hirvonen, T., Takalo, R., Heiskanen, A., Satomaa, T., Natunen, S., Lehtonen, S., Hakkarainen, T., Korhonen, M., Laitinen, S., Valmu, L., Lehenkari, P., 2013. Cell surface structures influence lung clearance rate of systemically infused mesenchymal stromal cells. Stem Cells 31, 317–326.

Reddy, L.H., Arias, J.L., Nicolas, J., Couvreur, P., 2012. Magnetic nanoparticles: design and characterization, toxicity and biocompatibility, pharmaceutical and biomedical applications. Chem. Rev. 112, 5818–5878.

Rowland, L.P., Shneider, N.A., 2001. Amyotrophic lateral sclerosis. N. Engl. J. Med. 344, 1688–1700.

Ruster, B., Gottig, S., Ludwig, R.J., Bistrian, R., Muller, S., Seifried, E., Gille, J., Henschler, R., 2006. Mesenchymal stem cells display coordinated rolling and adhesion behavior on endothelial cells. Blood 108, 3938–3944.

Sahay, G., Alakhova, D.Y., Kabanov, A.V., 2010. Endocytosis of nanomedicines. J. Control. Release 145, 182–195.

Schrepfer, S., Deuse, T., Reichenspurner, H., Fischbein, M.P., Robbins, R.C., Pelletier, M.P., 2007. Stem cell transplantation: the lung barrier. Transplant. Proc. 39, 573–576.

Shah, N.B., Vercellotti, G.M., White, J.G., Fegan, A., Wagner, C.R., Bischof, J.C., 2012. Blood-nanoparticle interactions and in vivo biodistribution: impact of surface PEG and ligand properties. Mol. Pharm. 9, 2146–2155.

Silani, V., Calzarossa, C., Cova, L., Ticozzi, N., 2010. Stem cells in amyotrophic lateral sclerosis: motor neuron protection or replacement? CNS Neurol. Disord. Drug Targets 9, 314–324.

Sitia, L., Paolella, K., Romano, M., Violatto, M.B., Ferrari, R., Fumagalli, S., Colombo, L., Bello, E., De Simoni, M.G., D'Incalci, M., Morbidelli, M., Erba, E., Salmona, M., Moscatelli, D., Bigini, P., 2014. An integrated approach for the systematic evaluation of polymeric nanoparticles in healthy and diseased organisms. J. Nanoparticle Res. 16, 1–16.

Souayah, N., Coakley, K.M., Chen, R., Ende, N., McArdle, J.J., 2012. Defective neuromuscular transmission in the SOD1 G93A transgenic mouse improves after administration of human umbilical cord blood cells. Stem Cell Rev. 8, 224–228.

Srivastava, A.K., Bulte, J.W., 2014. Seeing stem cells at work in vivo. Stem Cell Rev. 10, 127–144.

Stagg, J., Galipeau, J., 2013. Mechanisms of immune modulation by mesenchymal stromal cells and clinical translation. Curr. Mol. Med. 13, 856–867.

Sutton, E.J., Henning, T.D., Pichler, B.J., Bremer, C., Daldrup-Link, H.E., 2008. Cell tracking with optical imaging. Eur. Radiol. 18, 2021–2032.

Tenuta, T., Monopoli, M.P., Kim, J., Salvati, A., Dawson, K.A., Sandin, P., Lynch, I., 2011. Elution of labile fluorescent dye from nanoparticles during biological use. PLoS One 6, e25556.

Uccelli, A., Moretta, L., Pistoia, V., 2008. Mesenchymal stem cells in health and disease. Nat. Rev. Immunol. 8, 726–736.

Uccelli, A., Benvenuto, F., Laroni, A., Giunti, D., 2011. Neuroprotective features of mesenchymal stem cells. Best Pract. Res. Clin. Haematol. 24, 59–64.

Uccelli, A., Milanese, M., Principato, M.C., Morando, S., Bonifacino, T., Vergani, L., Giunti, D., Voci, A., Carminati, E., Giribaldi, F., Caponnetto, C., Bonanno, G., 2012. Intravenous mesenchymal stem cells improve survival and motor function in experimental amyotrophic lateral sclerosis. Mol. Med. 18, 794–804.

Vaegler, M., Maerz, J.K., Amend, B., da Silva, L.A., Mannheim, J.G., Fuchs, K., Will, S., Sievert, K.D., Stenzl, A., Hart, M.L., Aicher, W.K., 2014. Labelling and tracking of human mesenchymal stromal cells in preclinical studies and large animal models of degenerative diseases. Curr. Stem Cell Res. Ther. 9, 444–450.

Viswanathan, S., Keating, A., 2011. Overcoming the challenges of conducting translational research in cell therapy. Front. Med. 5, 333–335.

Wang, P., Moore, A., 2012. Molecular imaging of stem cell transplantation for neurodegenerative diseases. Curr. Pharm. Des. 18, 4426–4440.

Willing, A.E., Garbuzova-Davis, S., Sanberg, P.R., Saporta, S., 2008. Routes of stem cell administration in the adult rodent. Methods Mol. Biol. 438, 383–401.

Wong, F.S., Chan, B.P., Lo, A.C., 2014. Carriers in cell-based therapies for neurological disorders. Int. J. Mol. Sci. 15, 10669–10723.

Zanotti, L., Sarukhan, A., Dander, E., Castor, M., Cibella, J., Soldani, C., Trovato, A.E., Ploia, C., Luca, G., Calvitti, M., Mancuso, F., Arato, I., Golemac, M., Jonjic, N., Biondi, A., Calafiore, R., Locati, M., D'Amico, G., Viola, A., 2013. Encapsulated mesenchymal stem cells for in vivo immunomodulation. Leukemia 27, 500–503.

Zhao, C.P., Zhang, C., Zhou, S.N., Xie, Y.M., Wang, Y.H., Huang, H., Shang, Y.C., Li, W.Y., Zhou, C., Yu, M.J., Feng, S.W., 2007. Human mesenchymal stromal cells ameliorate the phenotype of SOD1–G93A ALS mice. Cytotherapy 9, 414–426.

Zoja, C., Garcia, P.B., Rota, C., Conti, S., Gagliardini, E., Corna, D., Zanchi, C., Bigini, P., Benigni, A., Remuzzi, G., Morigi, M., 2012. Mesenchymal stem cell therapy promotes renal repair by limiting glomerular podocyte and progenitor cell dysfunction in adriamycin-induced nephropathy. Am. J. Physiol. Ren. Physiol. 303, F1370–F1381.